Electronic Supplementary Material (ESI) for Energy & Environmental Science.
This journal is © The Royal Society of Chemistry 2018

Use of poly-cation oxides to lower the temperature of two-step thermochemical water splitting

Electronic Supplementary Information

Shang Zhai[a], Jimmy Rojas[a], Nadia Ahlborg[b], Kipil Lim[b,c],
Michael F. Toney[c], Hyungyu Jin[a,f,*], William C. Chueh[b,d,e,*], Arun Majumdar[a,d,*]

[a] Department of Mechanical Engineering, Stanford University, Stanford, CA 94305, USA.

[b] Department of Materials Science and Engineering, Stanford University, Stanford, CA 94305, USA.

[c] Stanford Synchrotron Radiation Lightsource, SLAC National Accelerator Laboratory, Menlo Park, CA 94025, USA.

[d] Precourt Institute for Energy, Stanford University, Stanford, CA 94305, USA.

[e] Stanford Institute of Materials and Energy Sciences, SLAC National Accelerator Laboratory, Menlo Park, CA 94025, USA.

[f] Department of Mechanical Engineering, Pohang University of Science and Technology (POSTECH), Pohang 37673, South Korea.

[*] Corresponding authors:
hgjin@postech.ac.kr; wchueh@stanford.edu; amajumdar@stanford.edu

1. Sample Synthesis

Solid-state synthesis

All reagents used in these experiments were used without further purification treatment. For the solid-state (SS) synthesis, reagents in powder forms were mixed. To synthesize $(FeMgCoNi)O_x$, for example, magnesium oxide (99.99%, Sigma-Aldrich), iron (II,III) oxide (99.997%, Alfa Aesar), cobalt (II,III) oxide (99.7%, Alfa Aesar) and nickel (II) oxide (99.99%, Sigma-Aldrich) with equimolar of cations were mixed for 1 min at 2000 rpm in a Vortex Mixer. The mixture was then transferred into an agate mortar and ground in acetone for 2 min. Calcinations were sequentially performed at 1000°C and 1350°C for 4 hours each (3°C/min between them), before a final cooling at 6°C/min to 500°C and a natural cooling thereafter. The sintered sample chunk was then broken and sieved (Fisherbrand stainless steel sieves) into 1.0~2.0 mm pieces for stagnation flow reactor. Powder sample was not used because fast gas flow in the reactor can blow away the powder from its holder. The remaining powder was used for quenching and X-ray characterizations, while the pieces were cycled in stagnation flow reactor explained below.

Sol-gel synthesis

For $(FeMgCoNi)O_x$, magnesium nitrate hexahydrate (99%, Sigma-Aldrich), iron(III) nitrate nonahydrate (≥98%, Sigma-Aldrich), cobalt(II) nitrate hexahydrate (≥98%, Sigma-Aldrich) and nickel(II) nitrate hexahydrate (crystalline, Sigma-Aldrich) with equimolar cations were dissolved in DI water with precursors:water = 1:4 in mass. EDTA (ethylenediamine tetraacetic acid, ACS, MP Biomedicals) and citric acid (≥99.5%, Sigma-Aldrich) were added to the solution with 60% and 75% the total molar amount of metal ions, respectively. (For example, if there was 1 mole of each metal cation, 2.4 mol EDTA and 3 mol citric acid would be added.) With 300 rpm stirring, ammonium hydroxide solution (28% - 30%, Fisher Chemical) was added until pH = 11, and a dark solution formed.

The resulting solution was stirred and heated on a hot plate at 200°C for about 5 hrs (gelation). The spin bar was removed and the temperature was increased to 300°C to dry the gel overnight, during which foaming happened and gel became almost solid. The beaker was then moved to a box furnace and heated at 300°C for 1 hr. The sample was ground into powder, transferred to an

alumina boat and went through the following calcination in air: 10°C/min until 800°C and 5°C/min until 1000°C, held there for an hour, 5°C/min until 800°C and then natural cooling.

Fig. S1 shows the sintering of the sol-gel (SG) samples when T_H exceeded the calcination temperature. Also compared is the morphology of the solid-state synthesized samples.

2. Reactors

TGA-GC

The simultaneous thermal analyzer NETZSCH STA 449 F3 Jupiter was used for thermochemical water splitting measurement. The system schematic is shown in **Fig. S2**. Cellkraft Humidifier P-2 provided 0 ~ 15.0 vol% humidified Argon mixture to the system. All gas lines containing water vapor were heated to ~90°C to avoid condensation.

Gas Chromatograph (Thermo Scientific, Trace GC Ultra + Trace GC Valve Oven) with thermal conductivity detector (TCD) was used to quantify H_2 in exhaust stream. Argon was used as carrier gas. Two columns are 25 m * 0.530 mm TRX Q – BOND and 10 m * 0.530 mm MS 5A PLOT 50 μm). Each measurement cycle takes 3 min, and H_2 production per gram of oxide is calculated by rectangular integration of the exhaust H_2 concentration minus background H_2 concentration (see **Table S1**). GC calibration gases are ultra-high purity (UHP) Ar, 54 ppm H_2 balance Ar and 1012 ppm H_2 balance Ar (Airgas). In this TGA-GC system, the uncertainty of GC quantification of H_2 yield is ± 0.1 mL-H_2/g/hour, considering ± 1.5 ppm uncertainty of GC quantification of H_2 concentration.

A Zirox ZR5 oxygen sensor measured O_2 partial pressure at the exhaust. The background pO_2 was found to be around 10 ppm (5 to 15 ppm) when UHP Ar was purged and 2 vol% water balance Ar was purged. (ZR5 sensor cannot tolerate water vapor that may condense at room temperature.) This small leak is from the TGA and the humidifier.

Thermogravimetry (TG) time-history data can be used to quantify O_2 evolutions. A “blank” experiment with no sample preceded each measurement, to identify the portion of mass change

associated with temperature and gas environment change; meanwhile the GC confirms background H_2 concentration. The sample mass increase during the water-splitting half-cycle could be theoretically assigned to incorporation of oxygen from steam into the sample and converted into H_2 yield (mL H_2 per gram of oxide). However, one should estimate the possible contribution to sample mass increase from accidental sample oxidation by background oxygen rather than steam. For example, during WS step, if 0.1 g of sample uptakes 10 ppm of O_2 in the background within total gas flow rate of 150 sccm, such contribution during 1 hour of WS will give an extra 0.13% TG increase beyond the sample mass change caused by water splitting. Even adding H_2 background may not easily remove such O_2 background; for example, at 600°C and 1 atm, combination reaction of 100 ppm H_2 and 20 ppm O_2 in Ar takes more than 10 seconds to reach equilibrium, based on a kinetics simulation[1].

Under the condition above, if one purely relies on TG to quantify H_2 production, the amount would be overestimated by as much as 1.8 mL-H_2/g. On the other, background O_2 is competing with steam to oxidize the sample, so the H_2 yield directly measured (with GC or else) under this condition would be smaller than an ideal case where no background O_2 is present.

Before each experiment, 150 sccm UHP Argon (Ar) was used to purge the system for about 1 hours (hr) until pO_2 stabilized. Then at about 160 sccm UHP Ar flow and 40°C/min ramp rate, the TGA furnace reached 1100°C; for T_H = 1300°C, a 20°C/min ramp rate was used for further heating due to TGA equipment requirement. At T_H, thermal reduction went on before it was cooled down at 50°C/min to T_L. Then a humidifier was included to inject H_2O into the purging Ar. In addition, background H_2 was injected to produce different ratios of H_2:H_2O partial pressures and water splitting reactions were studied. Gas composition details for different H_2:H_2O during water splitting are shown in **Table S1**. Subsequently, UHP Ar was used to purge for 5 min before the next cycle to drive away residual H_2 and H_2O.

Table S2 shows the comparison of TG derived H_2 production with direct GC quantification results. When background H_2 is high enough, the background O_2 effect mentioned above is negligible.

Stagnation flow reactor

Kinetic experiments were performed using a custom-built stagnation flow reactor, shown schematically in **Fig. S4a**. Approximately 200 mg of solid-state synthesized sample was placed in a porous zirconia fiber cup, which rested at the bottom of a vertical, close-one-end, alumina process tube. As in the TGA, the samples were first rapidly heated to 1300°C (ramping to 1270°C at 200°C/min and to 1300°C at 20°C/min) using an infrared furnace (ULVAC-Riko, Tokyo, Japan) under 200 sccm of flowing argon (UHP), then rapidly cooled to 800°C (ramping to 830°C at 200°C/min and to 800°C at 20°C/min). A Nafion-membrane humidification system (Cellcraft, Stockholm, Sweden) was used to inject a mixture of 24.2% H_2O and 0.0224% H_2 (balance gas argon) into the reactor with a total flow rate of 200 sccm. The reaction pressure is approximately 1 bar. A Prima BT Mass Spectrometer (Thermo Fisher Scientific, Waltham, MA) was used to quantify the concentrations of oxygen and hydrogen in the exhaust gas stream. The measured concentration, shown in **Fig. S4b**, is multiplied by the total gas flow rate (less the known flow rate of H_2 during the water-splitting step) gives the rate at which these gases were generated during each half-cycle. **Fig S5** shows the repeatability of the experiment over nine cycles.

For mass spectrometer, mass 32 (oxygen) and 2 (hydrogen) signals were calibrated by flowing known concentrations of each gas in argon and measuring the corresponding mass signals to form a calibration curve. Without a sample, it was observed during water-splitting conditions, both the mass 32 and mass 2 signals were higher than in pure argon; such signal elevations were attributed to water fragmentation. These backgrounds were subtracted from experimental data by averaging the measured values of several "blank" experiments, in which the reactor was bypassed and the process gases were flowed directly into the mass spectrometer. The error bars in O_2 and H_2 quantification represent the background drift from multiple "blank" runs multiplied by flow rate and time.

3. Quenching

CTF 17/300 CARBOLITE tube furnace, along with CellKraft Humidifier P-10, were used as a reactor. Solid-state synthesized samples were ground with mortar and pestle into powder and went through thermal reduction and/or water splitting step(s) and finally quenched under Ar immediately. X-ray characterizations were done on such quenched samples. For a thermal

reduction quench, for instance, 100 sccm ultra-high purity Ar was purged into the tube furnace at 100°C until the pO_2 sensor showed ~10 ppm. The furnace was then ramped up to T_H at 5°C /min, and after 30 min, the alumina boat containing the sample was pushed from the hot zone to the (actively) cooled upstream side of the furnace in 1 second. To achieve this, the Ar flow rate was increased to 600 mL/min to avoid back-flow from atmosphere, and then an alumina rod was inserted into the tube through a downstream Ultra Torr fitting previously plugged. Afterwards, it was plugged again. In a similar fashion, for a water splitting quenching test, the furnace would be cooled to T_L after thermal reduction step and 10% humidified Ar (without H_2 background) would be purged for 1 hr. The same quenching process would take place afterwards.

4. Characterizations

X-ray diffraction

Bruker D8 Advance X-ray diffractometer was used to collect powder diffraction patterns (XRD) using Cu K_α radiation over a 2θ range of 20° to 90° (step size of 0.02° for 2θ, scan step of 94.5 sec, fixed divergence slit of 0.6°, and generator at 40 mA and 40 kV.) Phase identification and Rietveld simulation were conducted with HighScore Plus software and PDF-4 (Powder Diffraction File).

For Rietveld refinement (see **Fig. S6**), magnetite (Fe_3O_4) and Fe_tO ($t \leq 1$) were used to simulate spinel and rocksalt phases of quenched PCO, respectively. Fe, Co and Ni have very similar atomic scattering factors and, when mixed, they are difficult to distinguish on XRD[2]. The fact that $t \leq 1$ is to account for two effects: 1) there is Mg on this site, 2) there are cation vacancies, similar as in nonstoichiometric FeO system, such as $Fe_{0.9}O$. In Rietveld refinement, it's hard to accurately refine both parameters, namely, Mg occupancy and cation vacancy occupancy, so we assumed it to be just Fe deficient Fe_tO. Thus the refined t value doesn't mean real stoichiometry of cation in the rocksalt phase, but rather the equivalent Fe occupancy leading to the same XRD pattern. So in the following approximate estimation of H_2 production, we use MO for rocksalt phase and M_3O_4 for spinel, where metal M has average atomic weight of Fe, Mg, Co and Ni, which is 49.4 g/mol.

The two-phase models are set as the **Tables S3** and **S4** show. Three sets of solid-state synthesis,

quenching (at four conditions) and XRD were repeated for $(FeMgCoNi)O_x$ and the results are in **Table S5**. The trend of phase ratio change is consistent among all three sets, as plotted in **Figure 4b**.

We can roughly estimate H_2 production of $(FeMgCoNi)O_x$ from the phase ratio swing refinement results. First we need to convert volumetric ratio to molar ratio. For rocksalt phase, the unit cell volume is about 4.215^3 Å^3 = 74.89 Å^3; there are 4 oxygen atoms in one unit cell; thus each oxygen corresponds to 74.89/4 = 18.72 Å^3 volume considering only anion sublattice. Similar calculation for spinel phase gives 18.35 Å^3, which is close to the rocksalt phase. Thus we can assume that the volumetric ratio is the same as the oxygen molar ratio between these two phases.

Starting from $(FeMgCoNi)O_x$ containing 1 mol of oxygen atoms, which is water-oxidized at 800°C, there is 0.666 mol of MO unit and 0.334 mol of $(1/4)M_3O_4$ unit according to **Table S5**. Suppose such oxide is thermally reduced to contain p mol of oxygen at 1300°C in Ar, and total amount of metal M which is p*(0.697+0.303*3/4) should equal to initial M amount which is 0.666+0.334*3/4 = 0.9165 mol. Thus we get p = 0.992 mol.

Such oxygen loss corresponds to (1-p) mol of H_2 production. H_2 production of $(FeMgCoNi)O_x$ is estimated to be 2.9 mL-H_2/g from the phase ratio swing between T_H = 1300°C and T_L = 800°C.

Similar calculation between T_H = 1100°C and T_L = 600°C gives an estimation of H_2 production of 1.8 mL-H_2/g. The H_2 yield estimation for 1300-800°C is similar to what **Figure 3a** presents, but the estimation for 1100-600°C is different from experimental results (we have not observed by GC any H_2 production at 1100-600°C condition). The reasons can be: 1) quenching was done in a tube furnace, which is different from the TGA and stagnation flow reactor; 2) the estimation above is based on a Rietveld refinement where only Fe and cation vacancy were considered, so the resulting phase ratio was a rough estimate; 3) the water splitting reaction in the quenching experiment did not have H_2 background as TGA measurements, potentially leading to more H_2 production and larger phase swing; 4) background O_2 can also oxidize the sample and give some phase swing; 5) oxygen nonstoichiometry isn't considered in such estimations, which could also be the mechanism of thermochemical water splitting of PCOs.

X-ray absorption near edge structure (XANES)

Fe K-edge, Co K-edge, Ni K-edge, and Zn K-edge XANES were measured at beamline 7-3 at Stanford Synchrotron Radiation Lightsource (SSRL). We used Si(220) double crystal monochromator, and transmission geometry was employed for XANES analysis. We measured metal foils together with samples to calibrate the energy. Powder samples were evenly spread onto the sticky Kapton tape. FeO, Fe_3O_4, Fe_2O_3, CoO, Co_3O_4, $LiCoO_2$, NiO, $NiFe_2O_4$, and La_2NiO_4 powder samples were purchased and measured for standard absorption edge of specific oxidation state of each element. The Athena software was used to calibrate the energy of each data set. **Figure S7** shows the XANES data for Co and Ni edge, whereas that for Fe is shown in **Figure 4c**.

SEM

Scanning electron microscopy (SEM) images were obtained on an FEI XL30 Sirion field-emission gun SEM at 5 kV. Lens astigmatism was addressed when necessary.

5. Calculation of Thermodynamic Limit of H_2 Production for LSM perovskites, CeO_2 and spinel ferrites

Thermochemistry data of LSM perovskites, e.g., LSM30 ($La_{0.7}Sr_{0.3}MnO_{3-\delta}$), and CeO_2 were taken from literature of CALPHAD simulation[3,4] and experiments[5–7]. Those data contain oxygen nonstoichiometry at various temperatures and pO_2 values, which can be used to calculate the thermodynamic limit of H_2 production in TWS through difference in equilibrium oxygen nonstoichiometries between thermal reduction and water splitting conditions. Specifically, the equilibrium oxygen nonstoichiometry at T_H was calculated for a pO_2 of 10^{-5} atm. This corresponds to a situation where the reactor pO_2 at the end of the oxygen release step is at this given value. Similarly, the equilibrium oxygen nonstoichiometry was calculated at T_L for a range of pH_2:pH_2O. Again, this corresponds to a situation where the reactor H_2:H_2O molar ratio is at this given value at the end of the hydrogen release step.

For example, for H_2:H_2O = 1:1045, the equilibrium constant of reaction H_2 (g) +1/2O_2 (g) = H_2O (g) is interpolated to be $10^{9.201}$ at 800°C (linear interpolation of the logarithms), giving equivalent pO_2 as $10^{-12.36}$ atm. Negative H_2 production (where the oxygen nonstoichomerty at T_L exceeded

that at T_H) is also calculated. We note that these calculations are somewhat different than that for a closed-system (i.e., batch reactor) typically done in literature, and reflect the fact that most experiments are carried out in an open-system (i.e., continuous flow reactor). **Tables S6** and **S7** provide the results of the thermodynamic limit calculations.

Thermodynamic limits of H_2 production by $NiFe_2O_4$ and $CoFe_2O_4$ were calculated based on the method of ΔH_O vs. ΔS_O plot analysis from Miller et al.[8] and data from CALPHAD simulations presented in [8,9]. The equilibrium stoichiometry results are as **Table S8** shows.

Supplementary Figures and Tables

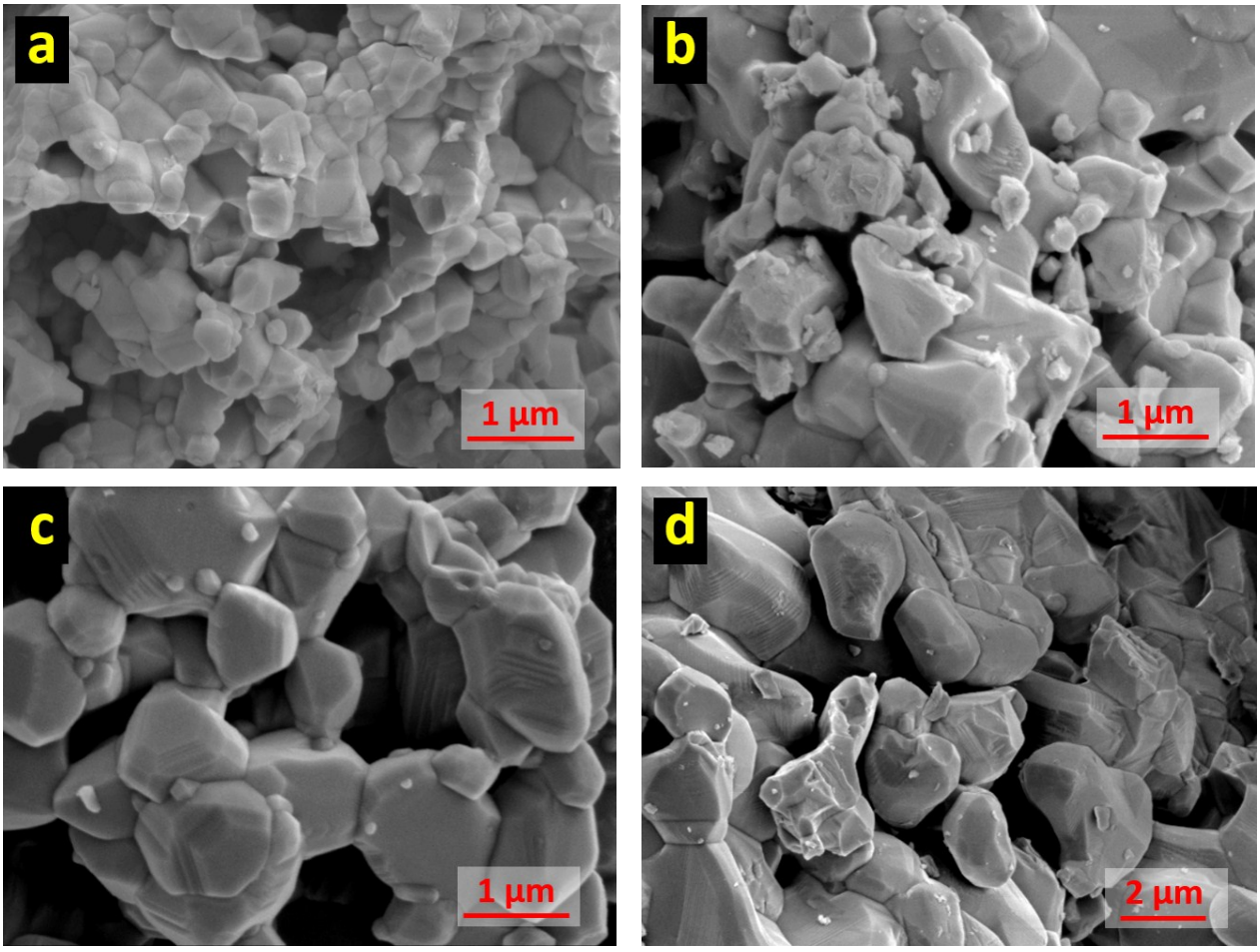

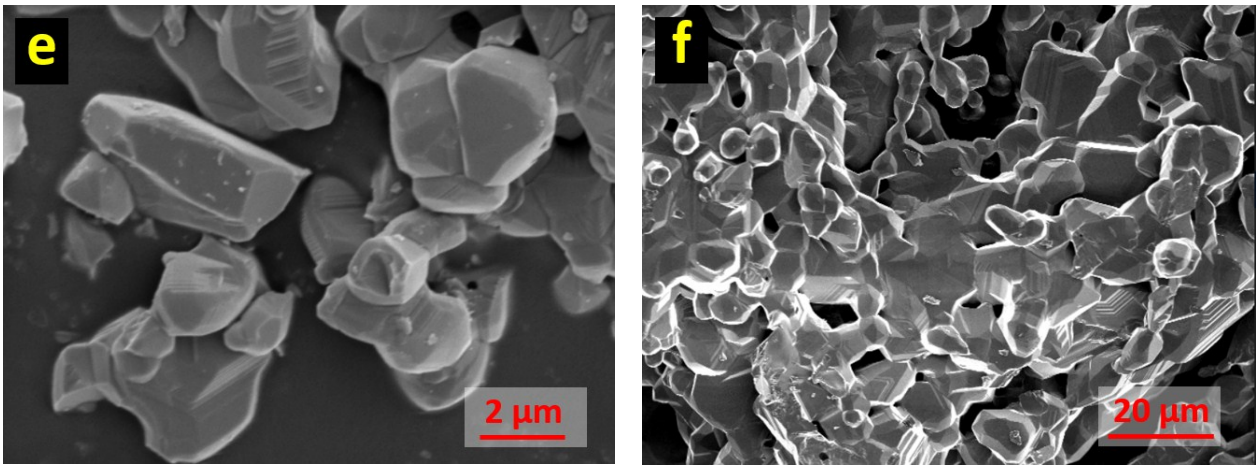

Fig. S1. Morphology of sol-gel and solid-state synthesized (FeMgCoNi)O_x. (**a**) Sol-gel synthesized (FeMgCoNi)O_x, using 1000°C calcination. (**b**) Sol-gel sample in (**a**) after going through two TWS cycles of T_H = 1100°C and T_L = 800°C; microstructure in (**a**) is sintered. (**c**) Sol-gel sample in (**a**) after going through ten TWS cycles of T_H = 1100°C and T_L = 800°C. (**d**) Sol-gel sample in (**a**) after going through two TWS cycles of T_H = 1300°C and T_L = 800°C; microstructure in (**a**) is strongly sintered. (**e**) Sol-gel sample in (**a**) after going through ten TWS cycles of T_H = 1300°C and T_L = 800°C. (**f**) Solid-state synthesized (FeMgCoNi)O_x, with 1350°C calcination, has >~10µm particle size. TWS cycles mentioned above have 0.5 hr of TR and 1 hr of WS.

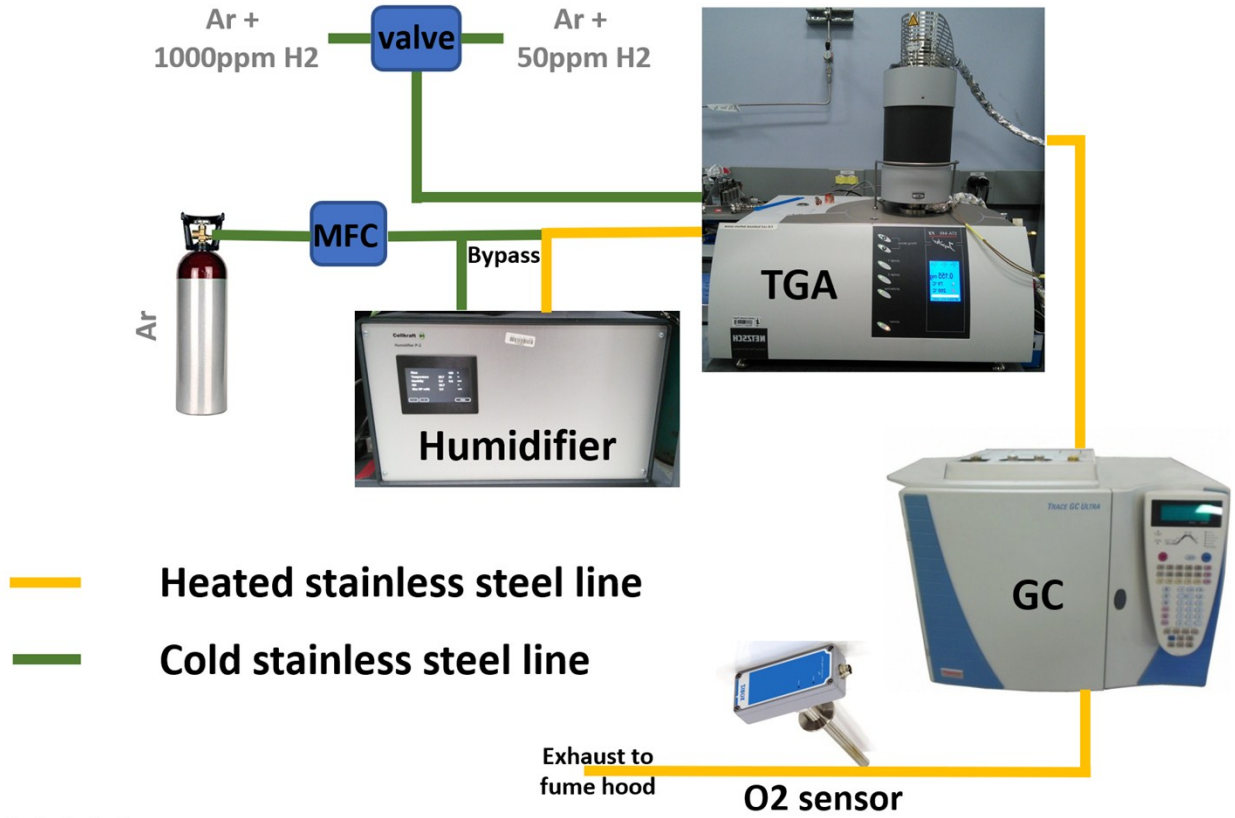

Fig. S2. TGA setup.

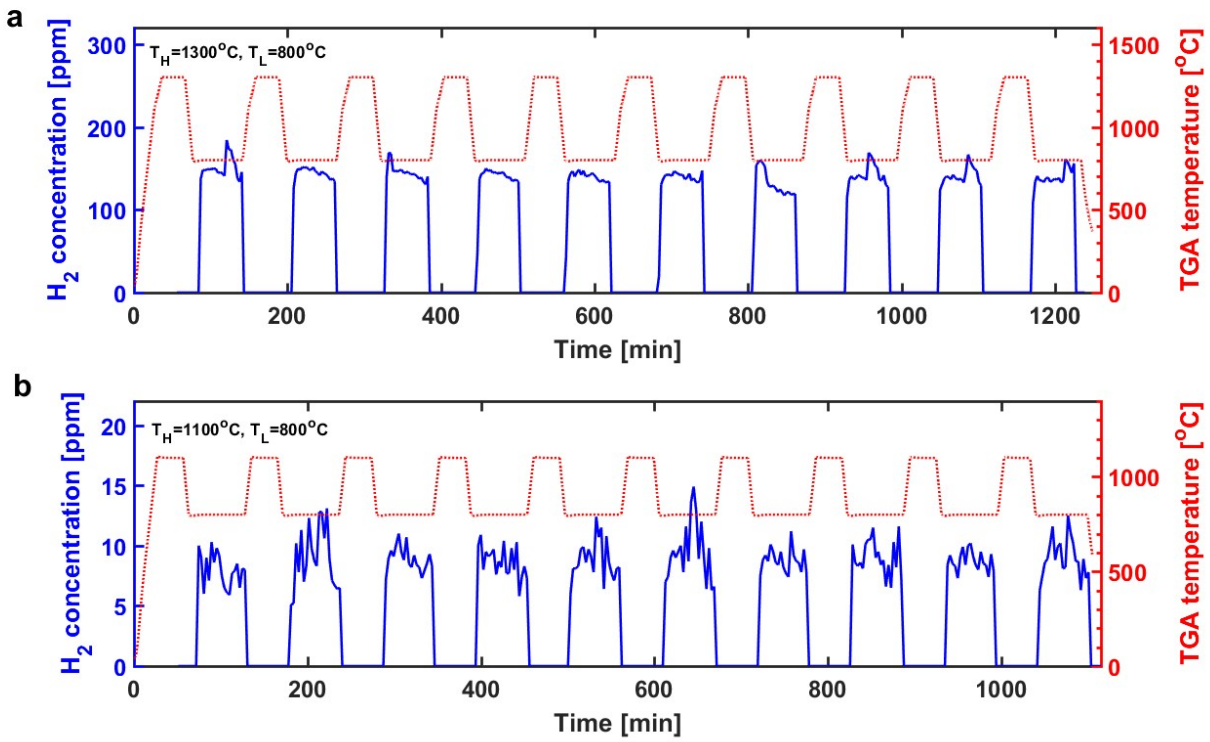

Fig. S3. H_2 concentration and temperature time-history for 10-cycle TWS tests of sol-gel synthesized (FeMgCoNi)O_x in TGA-GC.. Cycles with T_H = 1300°C and T_L = 800°C have 91 ppm H_2 background during water splitting steps; cycles with T_H = 1100°C and T_L = 800°C have 4.5 ppm H_2 background during water splitting steps. Instability of humidity in purge gas induced instability of H_2 concentration besides the noise of GC.

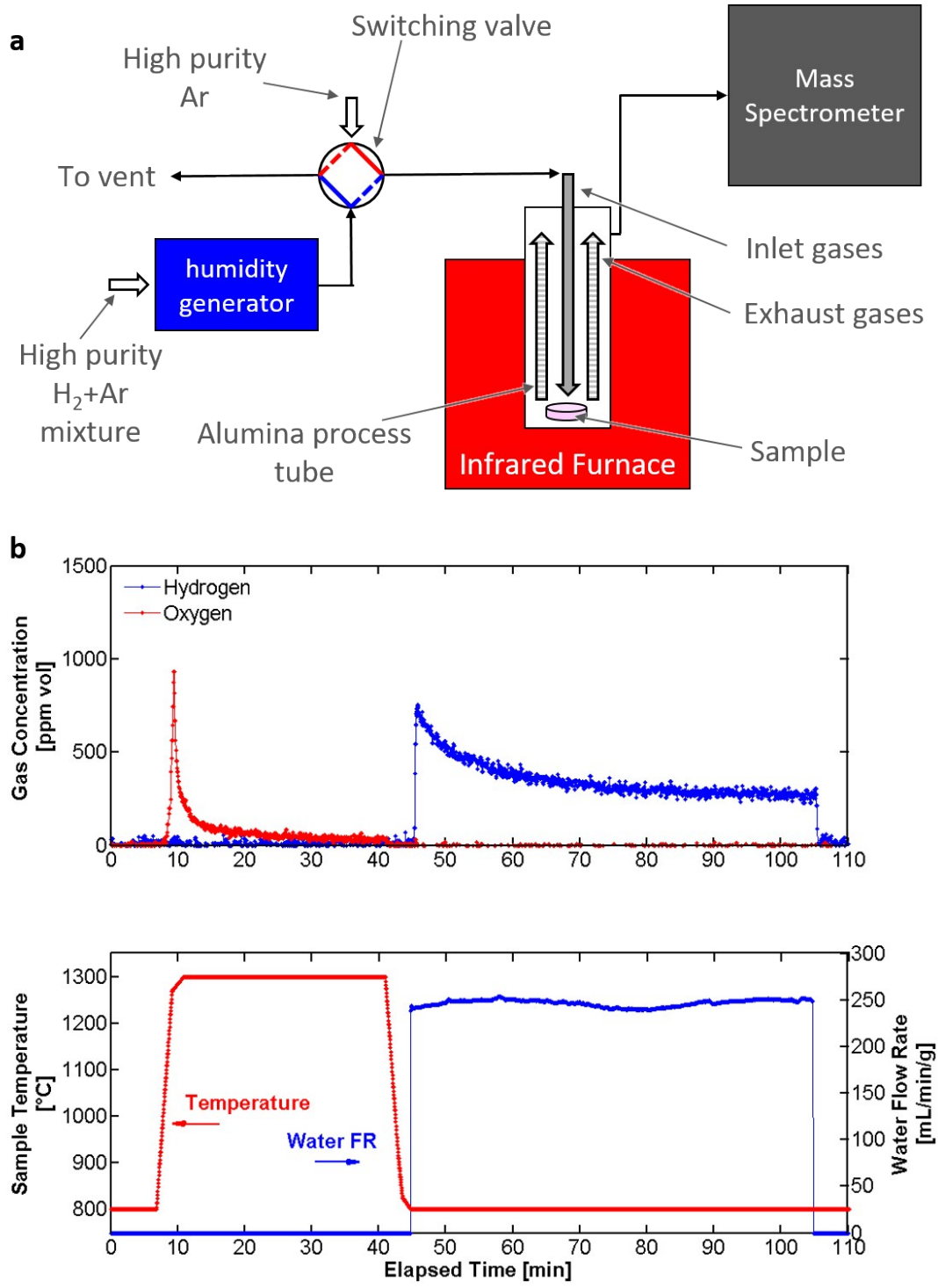

Fig. S4. Stagnation flow reactor setup and example of raw cycling data. (**a**) Schematic of stagnation flow reactor and gas delivery system. (**b**) Example raw concentration and temperature data used to generate kinetic curves shown in **Figure 3d**.

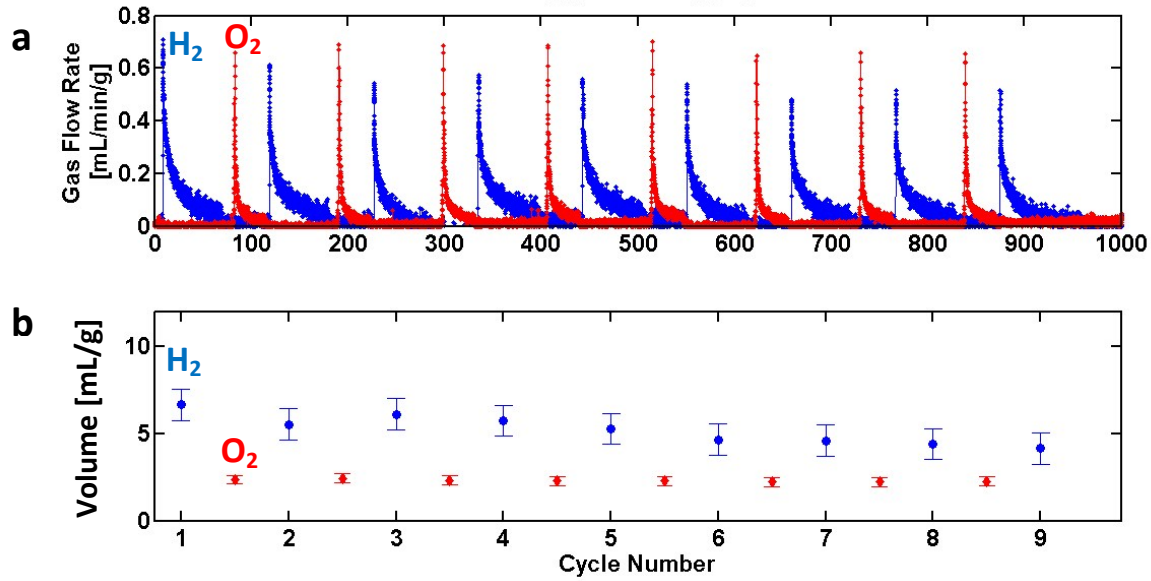

Fig. S5. Kinetic cycling data from stagnation flow reactor. (**a**) Nine thermochemical water-splitting cycles for equimolar $(FeMgCoNi)O_x$ synthesized by a solid-state route. The first oxygen release half-cycles are not shown because data recording began during the first water-splitting step. (**b**) Gas volume produced in each half-cycle. T_H = 1300°C and T_L = 800°C with H_2:H_2O = 10^{-3}.

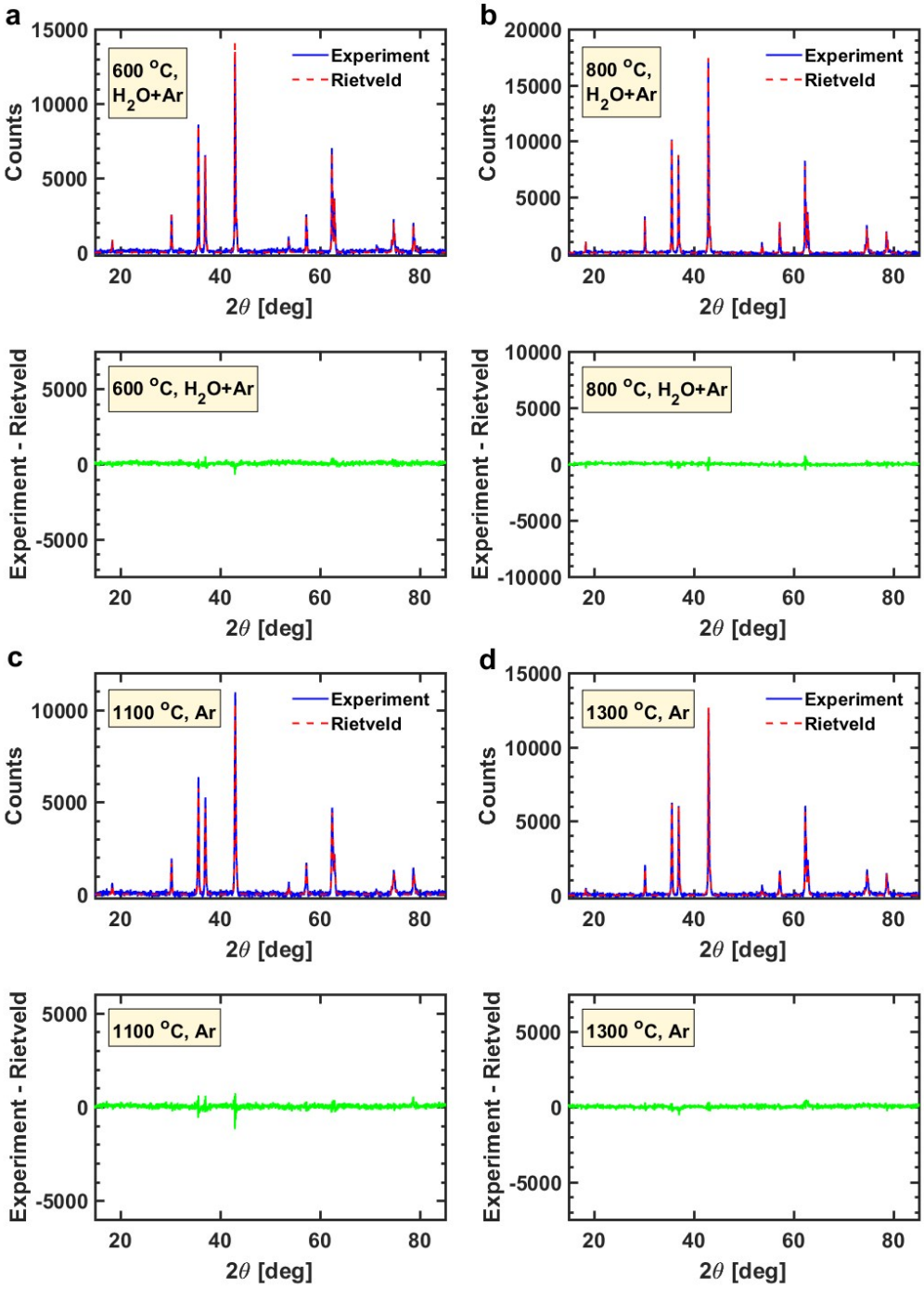

Fig. S6. Rietveld refinement results and difference plots for one set of quenched (FeMgCoNi)O_x.

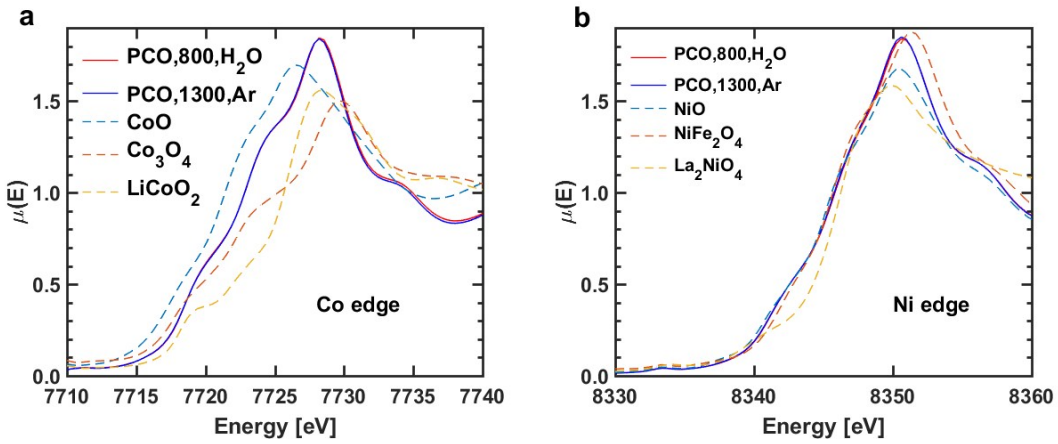

Fig. S7. X-ray absorption near edge structure (XANES) result for the Co and Ni edges of quenched (FeMgCoNi)O_x. In contrast to Fe, Co and Ni are essentially "inert" in the redox cycles.

Table S1. Water splitting environments for various H_2:H_2O ratios

a. T_H = 1300°C and T_L = 800°C

Total flow rate [sccm]	**Background H2 [ppm]**	**H_2O [%]**	**$p(H_2O)/p(H_2)$**
166	90.5	9.47	1045
165	121	6.06	500
164	214	5.31	248
165	383	3.96	104

b. T_H = 1100°C and T_L = 800°C

Total flow rate [sccm]	**Background H2 [ppm]**	**H_2O [%]**	**$p(H_2O)/p(H_2)$**
166	4.5	9.47	20909
162	9.2	6.92	7481
162	10.8	3.97	3684
164	16.4	3.30	2009

Table S2. Comparison of TG derived H_2 production with direct GC quantification results, for the 2nd TWS cycle.

Sample	Temperature	TR time	WS time	H_2:H_2O during WS	TGA derived, mL-H_2/g	GC, mL-H_2/g
$(FeMgCoNi)O_x$	1100-800°C	30 min	1 hr	1:20909	0.56	0.32
		5 hrs	5 hrs		2.78	1.42
	1300-800°C	30 min	1 hr	1:1045	3.39	2.97
		5 hrs	5 hrs		9.32	10.09

Table S3. Spinel phase settings

Space group: Fd-3m					
Atom	**Wyckoff positions**	**x**	**y**	**z**	**Occupancy**
Fe1	8b	0.375	0.375	0.375	1
Fe2	16c	0	0	0	1
O1	32e	0.2445	0.2445	0.2445	1

Table S4. Rocksalt phase settings

Space group: Fm-3m					
Atom	**Wyckoff positions**	**x**	**y**	**z**	**Occupancy**
Fe1	4a	0	0	0	t
O1	4b	0.5	0.5	0.5	1

Table S5. Rietveld refinement results of quenched $(FeMgCoNi)O_x$

Batch #	Sweep gas	T_{quench} [°C]	Rocksalt phase			Spinel phase		Goodness-of-fit
			Volumetric Ratio	t (in Fe_tO)	Lattice param. [Å]	Volumetric Ratio	Lattice param. [Å]	
1	H_2O+Ar	600	0.66(1)	0.750(3)	4.21454(5)	0.338(3)	8.3731(1)	1.59
		800	0.66(1)	0.751(3)	4.21527(6)	0.342(3)	8.3754(1)	1.17
	Ar	1100	0.67(1)	0.766(3)	4.21413(5)	0.327(2)	8.3761(1)	1.40
		1300	0.70(1)	0.772(3)	4.21578(9)	0.301(3)	8.3820(3)	1.26
2	H_2O+Ar	600	0.67(1)	0.738(3)	4.21379(4)	0.334(2)	8.3693(1)	1.51
		800	0.67(1)	0.718(4)	4.21411(9)	0.327(4)	8.3694(2)	1.42
	Ar	1100	0.68(1)	0.745(3)	4.21264(5)	0.319(3)	8.3759(1)	1.43
		1300	0.70(1)	0.742(3)	4.2150(1)	0.305(4)	8.3766(3)	1.29
3	H_2O+Ar	600	0.67(1)	0.758(4)	4.21449(7)	0.333(4)	8.3684(2)	1.11
		800	0.68(1)	0.771(4)	4.21868(6)	0.322(4)	8.3735(1)	1.05
	Ar	1100	0.68(1)	0.777(5)	4.2134(1)	0.318(5)	8.3704(3)	1.16
		1300	0.70(1)	0.764(5)	4.2178(1)	0.300(4)	8.3768(3)	1.03

Table S6. Thermodynamic H_2 yields (unit: mL/g) of CeO_2 and LSM at T_H = 1300°C with pO_2 = 10^{-5} atm and T_L = 800°C with various H_2O:H_2 ratios. Data sources are noted in the 2nd row. Negative H_2 production means sample consumes H_2 in background and gets further reduced in the corresponding water splitting condition.

$p(H_2O)/p(H_2)$	**LSM20**	**LSM30**		**LSM40**		**CeO_2**
	Bork[3]	Bork[3]	Tagawa[6] and Scheffe[7]	Bork[3]	Tagawa[6] and Scheffe[7]	Panlener[5] and Zinkevich[4]
1045	0.77	1.58	2.67	1.62	4.55	1.41
500	0.58	0.59	2.08	-0.51	2.43	1.40
248	0.10	-0.59	1.09	-2.73	0.40	1.38
104	-0.87	-2.57	-0.69	-5.06	-2.13	1.35

Table S7. Thermodynamic H_2 yields (unit: mL/g) of CeO_2 and LSM at T_H = 1100°C with pO_2 = 10^{-5} atm and T_L = 800°C with various H_2O:H_2 ratios. Data sources are noted in the 2nd row. Negative H_2 production means sample consumes H_2 in background and gets further reduced in the corresponding water splitting condition.

$p(H_2O)/p(H_2)$	**LSM20**	**LSM30**		**LSM40**		**CeO_2**
	Bork[3]	Bork[3]	Tagawa[6] and Scheffe[7]	Bork[3]	Tagawa[6] and Scheffe[7]	Panlener[5] and Zinkevich[4]
20909	0.10	0.20	0.40	0.71	1.54	0.18
7481	0.10	0	0.20	-0.40	0.53	0.17
3684	0	-0.20	0	-1.52	-0.59	0.16
2009	0	-0.49	-0.20	-2.93	-1.9	0.15

Table S8. Thermodynamic equilibrium oxygen stoichiometry for $NiFe_2O_4$ and $CoFe_2O_4$.

Stoichiometric Material	$NiFe_2O_4$	$CoFe_2O_4$
T_H = 1300°C and $pO_2 = 10^{-5}$ atm	$NiFe_2O_{3.87}$	$CoFe_2O_{3.87}$
T_L = 800°C and H_2:H_2O = 1 : 10^3	$NiFe_2O_{3.97}$	$CoFe_2O_{3.975}$
T_H = 1100°C and $pO_2 = 10^{-5}$ atm	$NiFe_2O_{3.97}$	$CoFe_2O_{3.998}$
T_L = 800°C and H_2:H_2O = 1 : 2.1×10^4	$NiFe_2O_4$	$CoFe_2O_4$

Supplementary References

1 J. Shao, 2018, Personal communication.

2 D. Carta, M. F. Casula, A. Falqui, D. Loche, G. Mountjoy, C. Sangregorio and A. Corrias, *J. Phys. Chem. C*, 2009, **113**, 8606–8615.

3 A. H. Bork, E. Povoden-Karadeniz and J. L. M. Rupp, *Adv. Energy Mater.*, 2017, **7**, 1601086.

4 M. Zinkevich, D. Djurovic and F. Aldinger, *Solid State Ionics*, 2006, **177**, 989–1001.

5 R. J. Panlener, R. N. Blumenthal and J. E. Garnier, *J. Phys. Chem. Solids*, 1975, **36**, 1213–1222.

6 H. Tagawa, in *Proceedings of the 5th International Symposium on Solid Oxide Fuel Cells (SOFC-V)*, Aachen, Germany, 1997.

7 J. R. Scheffe, D. Weibel and A. Steinfeld, *Energy & Fuels*, 2013, **27**, 4250–4257.

8 J. E. Miller, A. H. McDaniel and M. D. Allendorf, *Adv. Energy Mater.*, 2014, **4**, 1300469.

9 I.-H. Jung, S. A. Decterov, A. D. Pelton, H.-M. Kim and Y.-B. Kang, *Acta Mater.*, 2004, **52**, 507–519.